JOURNAL OF GEOPHYSICAL RESEARCH, VOL. 114, A08214, doi:10.1029/2009JA014155, 2009

Effect of frequency modulation on whistler mode waves in the magnetosphere

A. V. Streltsov,[1] M. Gołkowski,[2] U. S. Inan,[2] and K. D. Papadopoulos[3]

Received 9 February 2009; revised 23 June 2009; accepted 26 June 2009; published 25 August 2009.

[1] We present results from numerical studies of whistler mode wave propagation in the Earth's magnetosphere. Numerical simulations, based on the novel algorithm, solving one-dimensional electron-MHD equations in the dipole coordinate system, demonstrate that the amplitude (and power) of the whistler mode waves generated by the ground-based transmitter can be significantly increased in some particular location along the magnetic field line (for example, at the equatorial magnetosphere) by the frequency modulation of the transmitted signal. The location where the amplitude of the signal reaches its maximum is defined by the time delay between different frequency components of the signal. Simulations reveal that a whistler mode wave with a discrete frequency modulation (where the frequency changes by a finite step) in the range from 1 to 3 kHz can be compressed as efficiently as a signal with a continuous frequency modulation when the frequency difference between components of the discrete-modulated signal is not greater than 100 Hz.

Citation: Streltsov, A. V., M. Gołkowski, U. S. Inan, and K. D. Papadopoulos (2009), Effect of frequency modulation on whistler mode waves in the magnetosphere, *J. Geophys. Res.*, *114*, A08214, doi:10.1029/2009JA014155.

1. Introduction

[2] The generation of ULF and VLF electromagnetic waves in the ionosphere by powerful ground-based HF transmitters and the propagation of these waves in the magnetosphere have been studied for more than three decades. Numerous advanced theoretical concepts related to this issue and results from a number of outstanding experiments have been reviewed by *Trakhtengertz et al.* [2000] and *Gurevich* [2007]. A particularly important concern of these studies is the dynamics of VLF waves in a whistler mode. These waves are important because of their ability to efficiently interact via cyclotron resonance with energetic electrons in the magnetosphere [*Nunn*, 1974; *Karpman et al.*, 1974; *Omura et al.*, 1991; *Trakhtengerts et al.*, 1996; *Nunn and Smith*, 1996; *Hobara et al.*, 2000]. These interactions can change the pitch angle of the energetic particles and precipitate them into the ionosphere. Therefore controlled injection of whistler mode signals into the magnetosphere can decrease the number of energetic particles and make the radiation environment safer for spacecraft, for example, inside the Earth's radiation belts [*Inan et al.*, 2003].

[3] The main problem with a practical use of these waves for the remediation of energetic electrons from the magnetosphere is that the wave-particle interactions are more efficient in the nonlinear regime, which depends on the wave amplitude/power. When this amplitude exceeds some particular threshold, the initial signal can be further amplified by interactions with energetic particles and trigger intense, secondary emissions [*Helliwell*, 1988]. Therefore it is important to develop the most efficient way to deliver electromagnetic power from the ionosphere to the equatorial magnetosphere, where the wave-particle interactions take place [*Trakhtengerts et al.*, 2004, 2007]. This issue is particularly important for the experiments conducted at the High Frequency Active Aurora Research Program (HAARP) facility in Alaska, where VLF signals are generated by the modulating of the ionospheric conductivity in the auroral electrojet region [*Papadopoulos et al.*, 2003; *Gołkowski et al.*, 2008], because this mechanism is not as efficient as a wave generation done with a very long VLF antenna on the ground, which was done in classic experiments at Siple Station, Antarctica [*Inan et al.*, 1985, 2003; *Helliwell*, 1988].

[4] In this paper, we present results from numerical studies of the effect of the frequency modulation of the whistler mode signal transmitted from the ionosphere on the wave amplitude and frequency spectra along the wave path in the magnetosphere. Our goal is to find the regime of frequency modulation which will maximize the wave amplitude in the equatorial magnetosphere, where wave-particle interactions take place. Effects of this frequency modulation scheme will be tested in future experiments conducted at HAARP.

2. Model

[5] VLF waves in the magnetospheric plasma can be described with electron magnetohydrodynamics (EMHD)

[1]Thayer School of Engineering, Dartmouth College, Hanover, New Hampshire, USA.
[2]STAR Laboratory, Stanford University, Stanford, California, USA.
[3]Department of Physics and Astronomy, University of Maryland, College Park, Maryland, USA.

0148-0227/09/2009JA014155$09.00

equations, where ions are considered to be immobile and electrons are treated as a cold fluid carrying current [*Helliwell*, 1965; *Gordeev et al.*, 1994]. The EMHD model considered in this paper consists of the electron momentum equation and Maxwell's equations

$$\frac{\partial \mathbf{v}}{\partial t} + (\mathbf{v}\cdot\nabla)\mathbf{v} = -\frac{e}{m_e}(\mathbf{E} + \mathbf{v}\times\mathbf{B}), \tag{1}$$

$$\nabla\times\mathbf{B} = \mu_0\mathbf{j}, \tag{2}$$

$$\nabla\times\mathbf{E} = -\frac{\partial \mathbf{B}}{\partial t}, \tag{3}$$

$$\nabla\cdot\mathbf{B} = 0. \tag{4}$$

The displacement current in Ampere's law is neglected. This is a so-called "quasilongitudinal" approximation of EMHD, which is valid when the wave circular frequency ω satisfies conditions $\omega_{HL} < \omega < \omega_{ce} \ll \omega_{pe}$, where ω_{HL} is the lower hybrid frequency; ω_{ce} is the electron gyrofrequency; and ω_{pe} is the electron plasma frequency [*Sazhin*, 1993].

[6] Using relation $\mathbf{j} = -en_e\mathbf{v}$, equations (1)–(4) can be reduced to three vector equations for the wave magnetic field, **B**, the electron fluid velocity **v**, and the electric field, **E**

$$\frac{\partial \mathbf{B}}{\partial t} = -\nabla\times\mathbf{E} \tag{5}$$

$$\mathbf{v} = -\frac{1}{\mu_0 ne}\nabla\times\mathbf{B} \tag{6}$$

$$\frac{m_e}{\mu_0 ne^2}\nabla\times\nabla\times\mathbf{E} + \mathbf{E} = -\frac{m_e}{e}(\mathbf{v}\cdot\nabla)\mathbf{v} - \mathbf{v}\times\mathbf{B} \tag{7}$$

To model whistler mode wave propagation in the Earth's magnetosphere, equations (5)–(7) are solved numerically in the dipole orthogonal coordinates, where the z axis is directed along the ambient magnetic field; the x axis lies in the meridional plane and is directed perpendicular to **z**, toward the center of the Earth; and the y axis completes the right hand coordinate system (x, y, z). This coordinate system adequately represents the ambient magnetic field starting in the ionosphere at latitudes corresponding to the location of Siple Station in Antarctica (L = 4.2) or the HAARP facility in Alaska (L = 4.9). The plot of this magnetic field line is shown in Figure 1.

[7] In this study, we consider the propagation of whistler mode waves in one spatial direction only (1D), namely along the ambient magnetic field. This type of propagation can happen when the wave is guided by the field-aligned density inhomogeneity or duct. Extensive theoretical studies of whistler mode waves guided by ducts have been summarized in several monographs [*Helliwell*, 1965; *Sazhin*, 1993; *Kondrat'ev et al.*, 1999]; and whistler mode waves in ducts have been observed in the Earth's magnetosphere [*Angerami*, 1970; *Scarf and Chapell*, 1973; *Carpenter and Anderson*, 1992; *Koons*, 1989; *Moullard et al.*, 2002] and in laboratory plasma devices [*Stenzel*, 1976; *Kostrov et al.*, 2000]. Therefore we conclude that the 1D case considered in this study is quite relevant to the whistler mode wave propagation in the real magnetosphere.

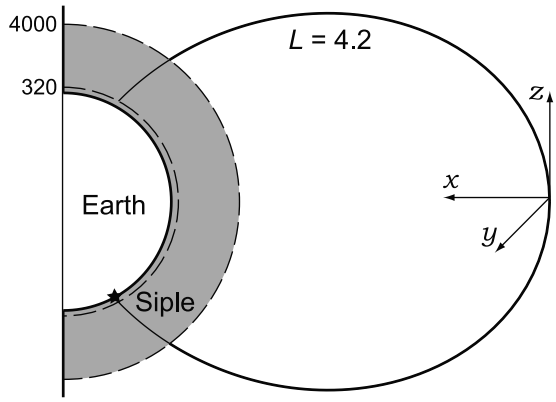

Figure 1. Dipole magnetic field line starting at Siple's magnetic latitude.

[8] In the 1D case, spatial derivatives in the z direction only are included in the model, and equations (4)–(6) can be reduced to 6 scalar equations for x and y components of the electric field, magnetic field, and the electron velocity:

$$\partial_t B_x = \partial_z\left(h_y E_y\right)/h_y h_z \tag{8}$$

$$\partial_t B_y = -\partial_z(h_x E_x)/h_x h_z \tag{9}$$

$$v_x = \beta\partial_z\left(h_y B_y\right)/h_y h_z \tag{10}$$

$$v_y = -\beta\partial_z(h_x B_x)/h_x h_z \tag{11}$$

$$E_x - \frac{\alpha}{h_y h_z}\partial_z\left(\frac{h_y}{h_x h_z}\partial_z(h_x E_x)\right) = -v_y B_0 \tag{12}$$

$$E_y - \frac{\alpha}{h_x h_z}\partial_z\left(\frac{h_x}{h_y h_z}\partial_z\left(h_y E_y\right)\right) = v_x B_0 \tag{13}$$

Here $\alpha = m_e/\mu_0 ne^2$; $\beta = 1/\mu_0 ne$ and $h_x = r^2/R_E \sin\theta\,(1 + 3\cos^2\theta)^{1/2}$; $h_y = r\sin\theta$; $h_z = r^3/R_E^2(1 + 3\cos^2\theta)^{1/2}$ are elements of the dipole metric tensor; θ is a colatitudinal angle; and r is a geocentric distance measured in R_E = 6371.2 km.

3. Background Parameters

[9] Parameters of the background plasma and ambient magnetic field used in this study are similar to the ones given by *Streltsov et al.* [2005]. The dipole magnetic field

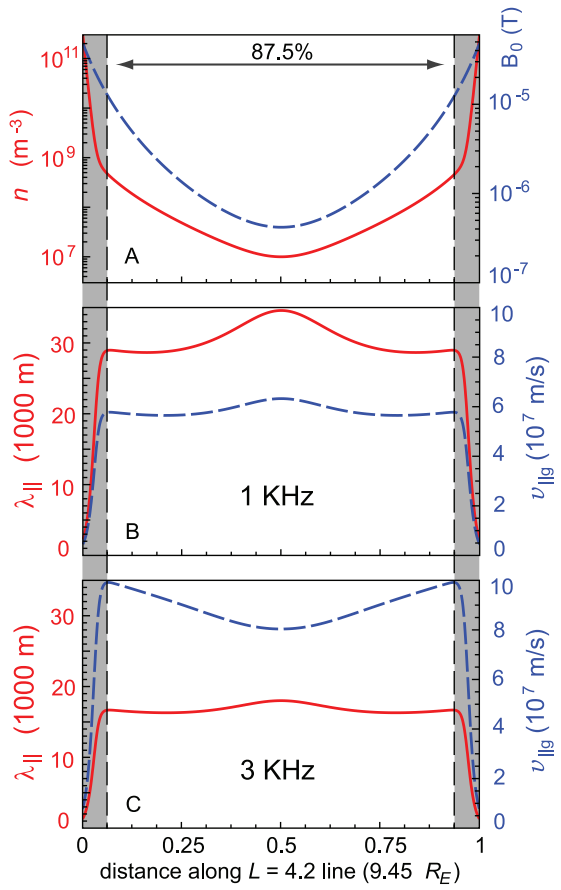

Figure 2. (a) Ambient geomagnetic field (dashed line) and the plasma density (solid line) along $L = 4.2$ magnetic field line. (b) Parallel wavelength (solid line) and the parallel group velocity (dashed line) of the whistler wave with frequency 1 kHz. (c) The same quantities for the whistler with frequency 3 kHz. Vertical dashed lines are drawn at 4000 km altitude.

is defined as $B_0 = B_* (1 + 3 \sin^2 \theta)^{1/2}/r^3$, where $B_* = 31000$ nT. The density profile along $\mathbf{B}_0$ is defined as

$$n_0(r) = \begin{cases} a_1 (r - r_1) + a_2, & r_1 < r < r_2 \\ b_1 e^{-20(r-r_2)} + b_2 r^{-3} + b_3, & r > r_2 \end{cases} \quad (14)$$

Here $r_1 = 1 + 110/R_E$, $r_2 = 1 + 270/R_E$; and the constants a_1, a_2, b_1, b_2, and b_3 are chosen to provide some prescribed values of density at three control locations along the ambient magnetic field line, namely 3×10^4 cm^{-3} at the altitude 110 km (near the ionospheric E-layer maximum), 3×10^5 cm^{-3} at the altitude 270 km (near the ionospheric F-layer maximum), and 10 cm^{-3} in the equatorial magnetosphere. Corresponding profiles of B_0 and n_0 along the $L = 4.2$ magnetic field line are shown in Figure 2a. Figure 2b shows profiles of the parallel wavelength, $\lambda_{||}$, and the parallel group velocity, $v_{||g}$, of the wave with frequency 1 kHz along the $L = 4.2$ magnetic field line. Figure 2c shows profiles of $\lambda_{||}$ and $v_{||g}$ for the wave with frequency 3 kHz. These quantities are calculated from the whistler mode dispersion relation, which, in the case of the wave propagating along B_0, is

$$\omega = \frac{\omega_{ce}}{\left(1 + \omega_{pe}^2/c^2 k_{||}^2\right)}, \quad (15)$$

and the definition of $v_{||g}$

$$v_{||g} = \frac{d\omega}{dk_{||}} = \frac{2k_{||}\omega_{ce}\omega_{pe}^2/c^2}{\left(k_{||}^2 + \omega_{pe}^2/c^2\right)^2}, \quad (16)$$

where ω_{pe} and ω_{ce} vary along the magnetic field line with B_0 and n_0.

[10] Figure 2 shows that for realistic parameters of the Earth's magnetosphere, $\lambda_{||}$ strongly decreases at the altitude below 4000 km. (This region is marked with the gray color and bounded with dashed vertical lines in Figure 2.) This effect is explained by the fact that the plasma density exponentially increases below this altitude toward the ionosphere. The small $\lambda_{||}$ means that at low altitudes, simulations should be performed with very high spatial resolution. Because whistler mode dynamics at low altitudes are not the main focus of this paper, the ionospheric boundary of the computational domain is set at an altitude of 4000 km above the ground, and the simulation domain represents ≈7/8 of the $L = 4.2$ magnetic flux tube. This assumption is quite reasonable for a theoretical study like this one; however, in case this code is used to model real experiments conducted at HAARP or another ground-based transmitter, a wave path below 4000 km altitude should be included in the model. The reason for this is the group velocity of whistler mode waves significantly decreases in this region, and this effect can cause a significant delay in the time of wave propagation from the ionosphere to the equator.

4. Numerical Technique

[11] Equations (8)–(13) are solved numerically inside the 1D computational domain (shown in Figure 1) by using the finite difference time domain (FDTD) technique. In this approach, partial derivatives in the z direction are approximated with second-order finite differences, and a third-order predictor-corrector algorithm is used to advance equations (8) and (9) in time. In particular, the four-step Adams-Bashforth method is used as a predictor, and the three-step Adams-Moulton method is used as a corrector *Burden and Faires* [2001]. The computational domain is discretized with uniform grids, and the grid used to calculate E_x and E_y is shifted by half of the distance between the two nearest nodes to the grid used to calculate B_x, B_y, v_x, and v_y. The grid used to simulate the electric field has 40,001 nodes and another grid has 39,999 nodes. Equations (12) and (13) for E_x and E_y are solved by using a direct solver with Dirichlet's type boundary conditions at the ionospheric ends of the domain. In simulations, the VLF signal is launched from one side of the domain by specifying the boundary

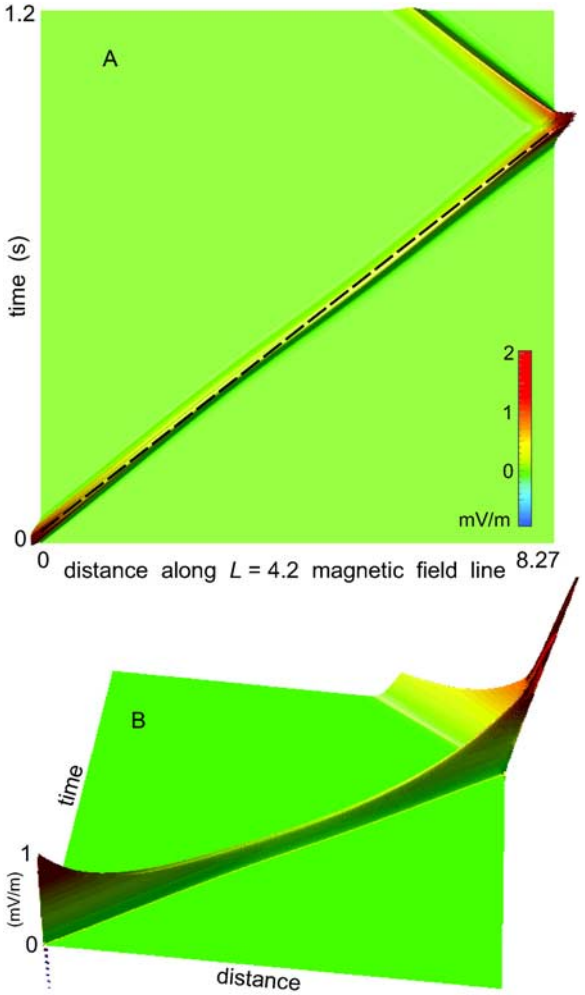

Figure 3. Amplitude of E_y in 20 ms pulse of 1 kHz wave traveling along $L = 4.2$ magnetic field line.

conditions $E_x(t) = E_0(t)\sin(\phi(t))$ and $E_y(t) = E_0(t)\cos(\phi(t))$, where $\phi(t)$ is the time-varying phase of the signal (it will be discussed in the next section) and

$$E_0(t) = E_* \begin{cases} t/t_R & t < t_R \\ 1 & t_R < t < t_I + t_R \\ (t_I + 2t_R - t)/t_R & t_I + t_R < t < t_I + 2\,t_R \\ 0 & t > t_I + 2\,t_R \end{cases} \quad (17)$$

Here $E_* = 1$ mV/m; $t_I = 20$ ms; and $t_R = 5$ ms. The boundary conditions for E at another boundary of the domain are $E_x(t) = E_t(t) = 0$. Physically, these conditions correspond to the situation when the ionosphere is a perfect conductor.

5. Results and Discussion

[12] Figure 3 shows results from the simulation of the propagation of a 20 ms pulse of 1 kHz whistler wave along the Siple magnetic field line from an altitude of 4000 km above the ground to the conjugate location. In particular, it shows the spatiotemporal behavior of the amplitude of E_y. The vertical axis in Figure 3a shows time, and the horizontal axis shows the distance along the magnetic field line. Because the group velocity of this wave changes along the $L = 4.2$ magnetic field line (see Figure 2b), the path of this signal in the time-distance plot shown in Figure 3a is not a straight line. To emphasize this effect, a straight, dashed line is added to Figure 3a. Figure 3b shows the same quantity in a different aspect. The main conclusion from Figure 3 is that the amplitude of the whistler waves in the equatorial region is significantly less than the wave amplitude near the ionosphere due to the divergence of the background magnetic field. This decrease in the amplitude is significant ($E_y = 0.2$ mV/m at the equator and $E_y = 1.0$ mV/m at the ionosphere), even if we assume that the whistler propagates exactly along B_0, which may happen if the wave is perfectly trapped inside the density duct [*Inan and Bell*, 1977; *Streltsov et al.*, 2007]. Since in the real situation this trapping is always imperfect (transverse gradients in the background plasma and magnetic field generally tend to "scatter" the wave across the ambient magnetic field) and other dissipative mechanisms (for example, wave-particle interactions, not considered in this model) take place, it is reasonable to expect that in the real magnetosphere, the wave amplitude will decrease from the ionosphere to the equatorial plane even more than is shown in Figure 3.

[13] One possible way to increase the amplitude of the whistler in the equatorial magnetosphere is to launch two pulses with different frequencies, one after another. If the wave frequency in the second pulse is higher than the frequency of the first pulse, then, because the group velocity of the higher frequency wave is larger than the group velocity of the lower frequency wave (for the parameters of the magnetosphere considered in this study, this state-

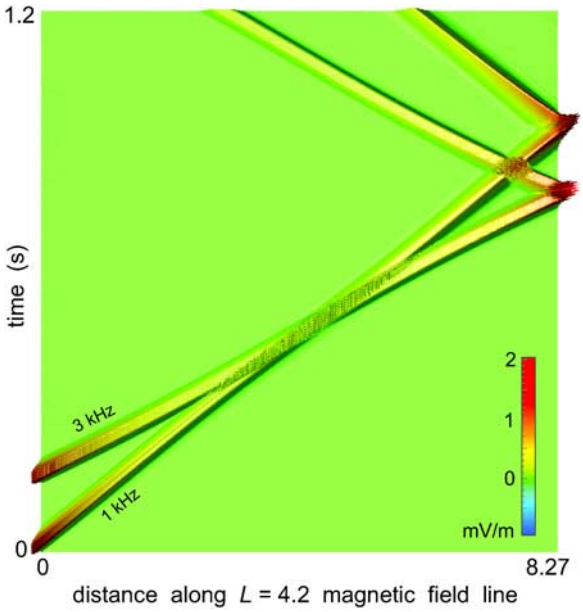

Figure 4. Amplitude of E_y in two 20-ms pulses of 1 kHz and 3 kHz waves traveling along $L = 4.2$ magnetic field line.

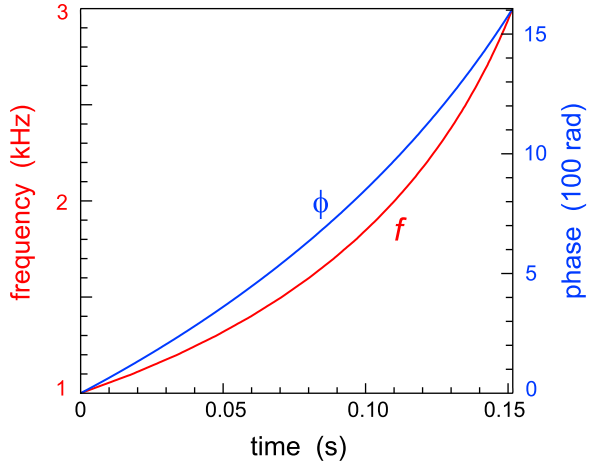

Figure 5. Variation in time of frequency f and phase ϕ in a signal focussing at the equator.

ment is correct for the waves in 1–3 kHz frequency range), the second pulse will "catch up" to the first one somewhere along the path, and the total field amplitude will increase in this location. The location on the magnetic field line where two pulses arrive simultaneously is controlled by the time when the second pulse is launched. This situation is illustrated in Figure 4 where the dynamics of two pulses of the same length of 20 ms but with frequencies 1 kHz and 3 kHz are shown. The time delay between pulses is equal to the difference between the traveling time of each signal to the equator, $T = \int_0^{\mathcal{L}} dt/v_{\|_g}$, where $\mathcal{L}$ is the distance along L = 4.2 magnetic field line from 4000 km altitude to the equator. For the parameters of the magnetosphere discussed in section 3, the time delay between the centers of 1 kHz and 3 kHz pulses is 0.152 s.

[14] This approach can be generalized further for a signal where the frequency changes in time from 1 kHz to 3 kHz according to the traveling time from the ionosphere to the equator of every harmonic within this frequency range. In order to construct such a signal, we calculate the traveltime of 21 signals with frequencies $f_k = 1 + (k - 1)$ 0.1 kHz (k = 1,. . ., 21) to the equator. These times are marked as t_1, t_2,. . ., t_{21}. The 21 time delays between these signals are defined as $t_{d1} = t_1 - t_1 = 0$, $t_{d2} = t_1 - t_2$, $t_{d3} = t_1 - t_3$,. . ., $t_{d21} = t_1 - t_{21}$. Therefore the signal which is expected to reach the equatorial magnetosphere at one instant in time should change the frequency in time at the ionospheric boundary as:

$$f(t) = \begin{cases} 0, & t > t_{d21} \\ f_k + \dfrac{t - t_{dk}}{t_{dk+1} - t_{dk}}(f_{k+1} - f_k), & t_{dk+1} > t > t_{dk} \end{cases} \quad (18)$$

The signal with frequency modulation defined by equation (18) can be launched into the simulation domain by specifying boundary conditions at one end of the domain as $E_x(t) = E_0 \sin(\phi(t))$ and $E_y(t) = E_0 \cos(\phi(t))$ with E_0 = 1 mV/m and $\phi(t) = 2\pi \int_0^t f(\tau)\, d\tau$, where $f(t)$ is defined by equation (18). Figure 5 shows plots of $f(t)$ and $\phi(t)$ calculated from equation (18) for the parameters of the magnetospheric plasma discussed in section 3.

[15] Results from simulations of propagation of the signal with modulated frequency and the signal with a constant frequency of 1 kHz are illustrated in Figure 6. Figure 6 shows an amplitude of E_y in these two whistler waves propagating along L = 4.2 magnetic field line. Figure 7 shows variations of E_y at three different locations along this magnetic field line during 0.15 s period of time. Right frames in Figure 7 show variations of E_y in the modulated signal, and left frames show variations of E_y in 1 kHz signal. The main conclusion from these results is that the focusing/compressing of the electromagnetic power at some

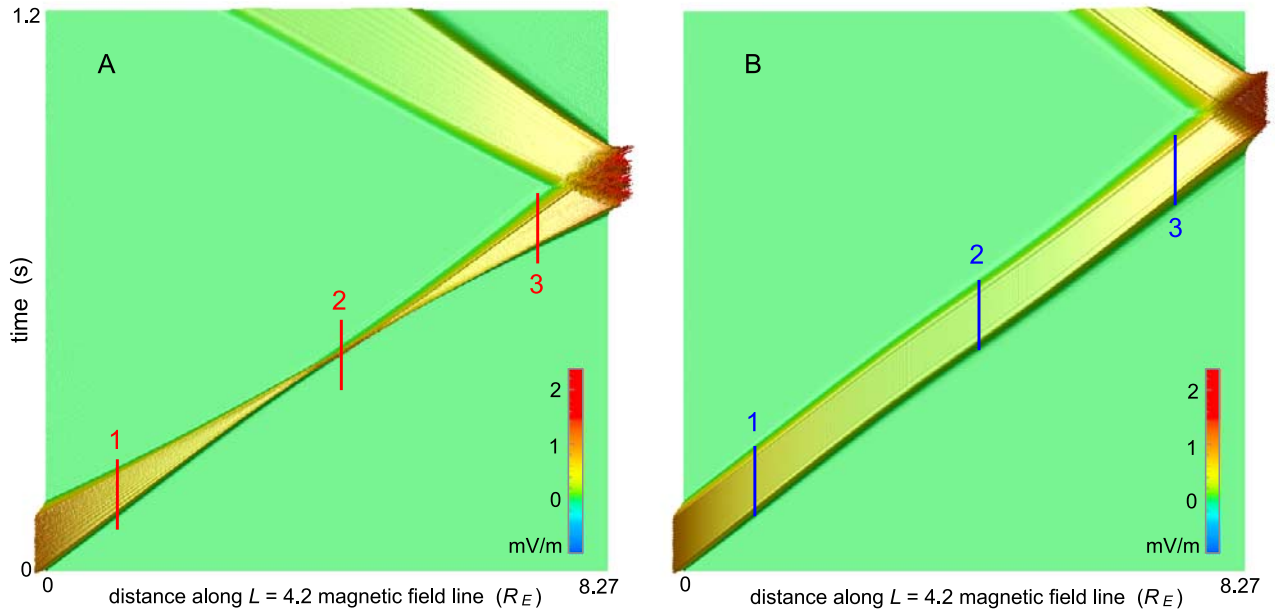

Figure 6. (a) Amplitude of E_y in a signal with frequency modulated from 1 to 3 kHz. (b) Amplitude of E_y in a signal with a frequency of 1 kHz.

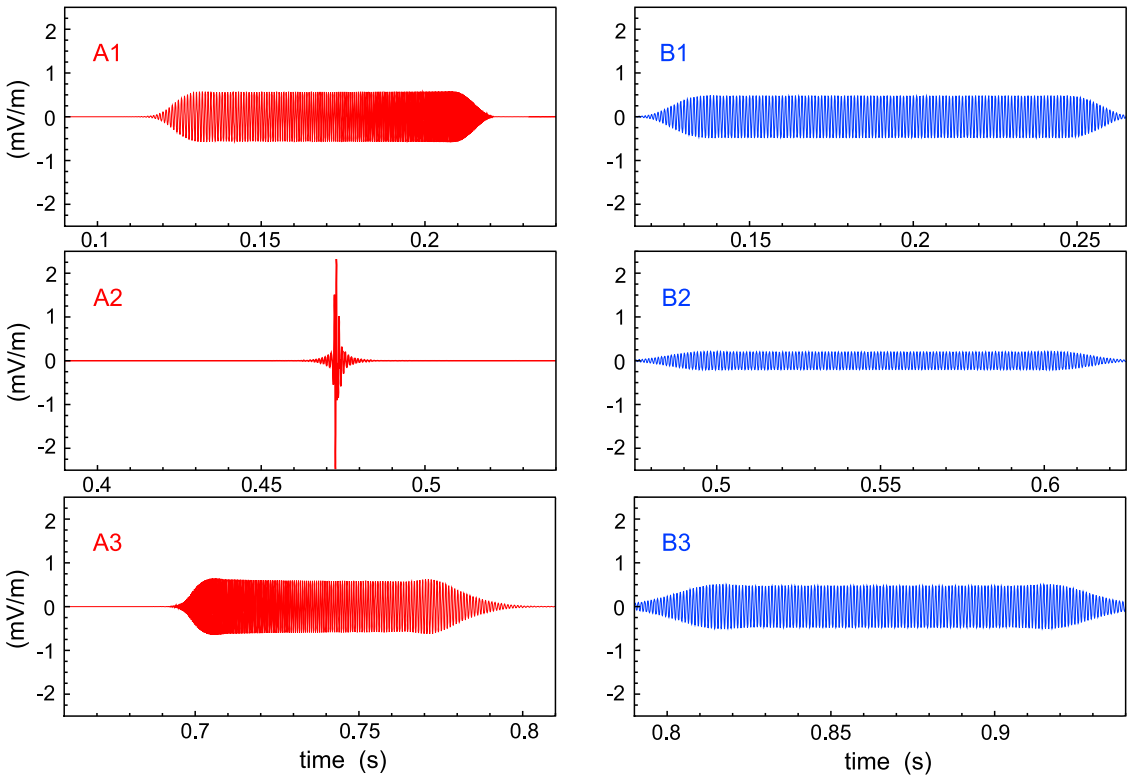

Figure 7. (left) E_y of the signal with frequency modulation at three locations along $L = 4.2$ magnetic field line shown in Figure 5. (right) E_y of 1 kHz signal at the same locations.

location along the ambient magnetic field line can indeed be achieved by the frequency modulation of the signal launched by the ground transmitter. Indeed, the amplitude of the modulated signal is 10 times larger than the amplitude of the uniform signal at the equatorial location (compare panels (A2) and (B2) in Figure 7), which means that instant power of the modulated signal at this location is 100 times larger than the instant power of the uniform signal. The second conclusion is that this focusing happens in the location predicted by the analysis based on the dispersion relation equation (16), which means that this relation adequately represents the dynamics of ducted whistler waves with frequencies from 1 to 3 kHz in the magnetosphere with parameters considered in this study.

[16] It should be mentioned here that whistler mode waves with the rate of frequency modulation of 1–2 kHz/s had been transmitted in many experiments at Siple Station, Antarctica [*Helliwell*, 1988]. In some experiments at HAARP, the rate of frequency modulation was ≈4.5–5 kHz/s. Our simulations suggest that in order to get a high-power signal at the equator, the rate of frequency modulation of waves in the 1 to 3 kHz frequency range should be of the order of 13 kHz/s.

[17] To understand in more detail the dynamics of the whistler wave with modulated frequency in the magnetosphere, we applied a Fourier transformation to the signals shown in the left frames in Figure 8. This transformation was applied to the signals within a time window of 9.83 ms length, sliding by 1.23 ms as a time step. The resulting dynamic spectrograms are shown in Figure 8 in frames A1, A2, and A3. The frame A0 shows the spectrogram of the signal taken at the boundary, near the transmitter. Figure 8 demonstrates that spectrograms of the signal taken at symmetrical points relative to the center of the domain (shown in frames (A1) and (A3)) are quite symmetrical indeed, and all the frequency components reach the center of the domain at the same moment of time (frame (A2)).

[18] It is interesting to compare spectra of the modulated signal at the boundary (near the transmitter) and at the center of the domain. This comparison is shown in Figure 9, which illustrates the energy spectral density of the signal measured at these two locations during 0.15 s time intervals. The main conclusion derived from Figure 9 is that the spectral width of the frequency modulated signal remains the same near the generator and at the equator, where the power of the signal increases. This result is quite expected from the linear character of our model. What is important to mention here (and what can be seen from Figure 8) is the fact that different frequency components of the signal appear near the transmitter at different instances in time (Figure 8(A0)), but all of them appear simultaneously at the equatorial region (Figure 8(A2)). Therefore this continuous regime of frequency modulation leads to a generation of high power, broadband signals in the magnetosphere.

[19] These signals may be important for some nonlinear processes of wave-particle interaction in the magnetosphere. However, results from a number of experiments at Siple Station, Antarctica, reveal that ducted broadband signals seldom demonstrate amplification or trigger intense secondary emissions [*Helliwell*, 1988]. In that sense, it is important to mention that the modulated signal becomes a true broadband signal only in one location along the magnetic field line (in our particular case, at the equator), and the amplification and triggering may occur before or after this point.

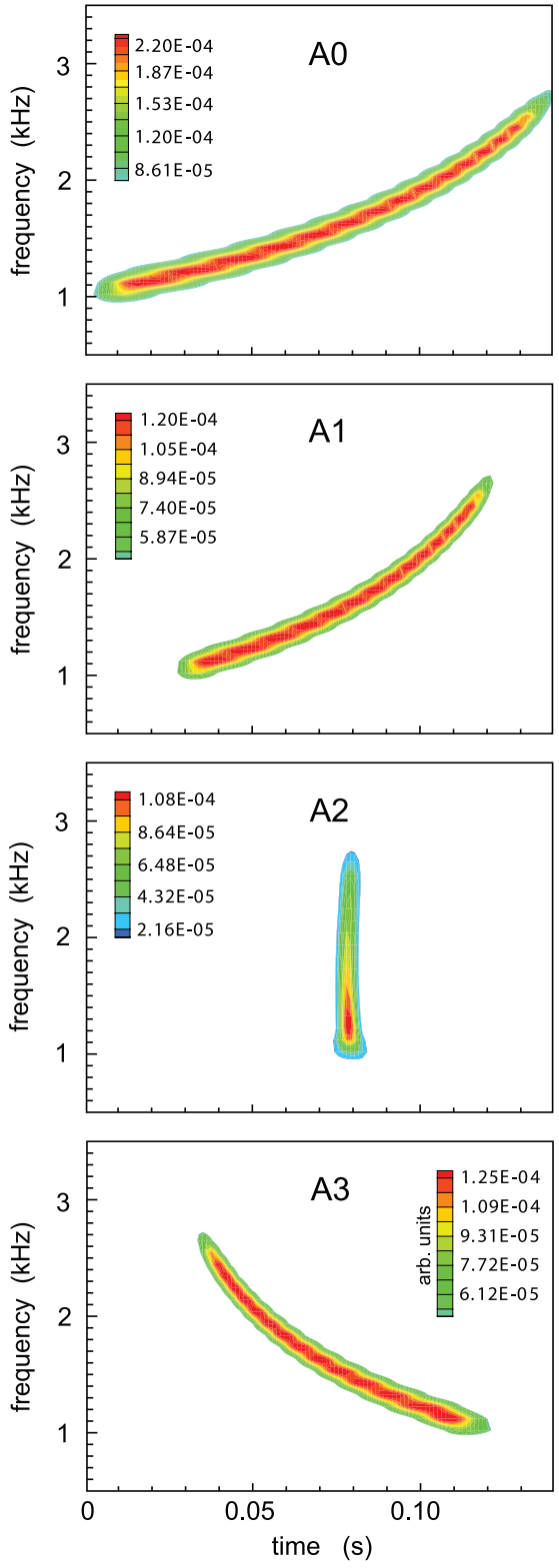

Figure 8. Temporal variation of the amplitude spectra of the modulated signal at the transmitter (A0) and at three locations along $L = 4.2$ magnetic field line shown in Figure 7 (A1, A2, and A3).

[20] Another consideration is that signal amplification and triggering were not observed in experiments at Siple Station when two signals with a frequency difference less than 20 Hz were launched together. At the same time, signals with a frequency difference of 100–200 Hz were amplified [*Helliwell*, 1988]. These results suggest that it may be reasonable to consider experiments where the frequency of the transmitted wave changes not in a smooth, continuous format, but rather in a discrete form, with a step of 100–200 Hz. The plot of this discrete frequency modulation is shown in Figure 10 with red lines.

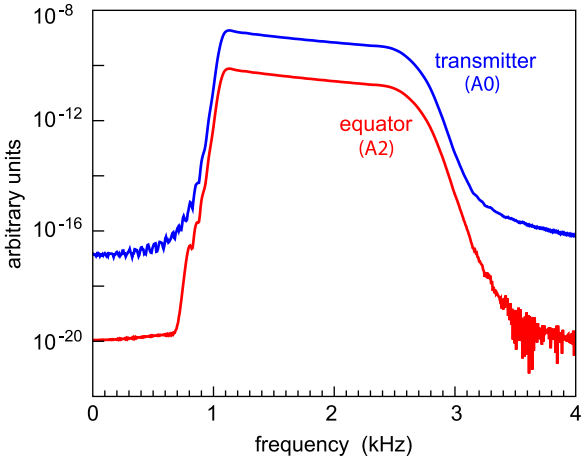

Figure 9. Energy spectral density of the modulated signal near the transmitter (A0) and at the equator (A2).

[21] Results from the simulation of the propagation of a discrete-modulated whistler mode wave are shown in Figure 11. Figure 11a shows the variation of amplitude of E_y in time and in space, as the signal propagates along $L = 4.2$ magnetic field line. Figure 11b shows variations of E_y at the equator during 0.15 s period of time. The same variation of the continuously modulated signal is shown in Figure 7(A1), and the maximum amplitude of E_y in these two cases is almost the same. Figure 11c shows the dynamic spectrogram of the signal shown in Figure 11b. This spectrogram is obtained by applying a Fourier transform within a time window of 39.32 ms length, sliding by 1.23 ms as a time step. Because this time window is 4 times larger

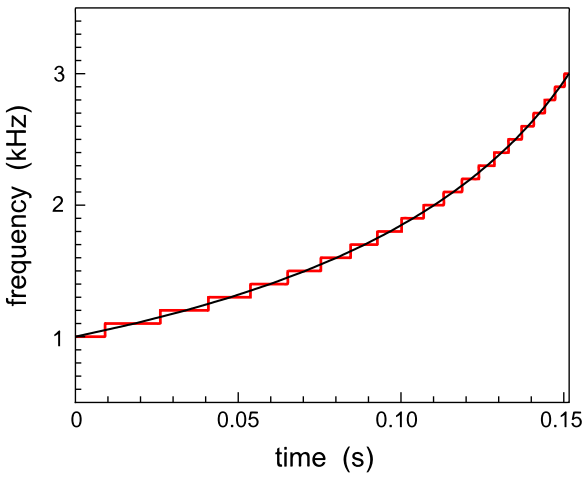

Figure 10. Discrete (with step of 100 Hz) and continuous frequency modulations.

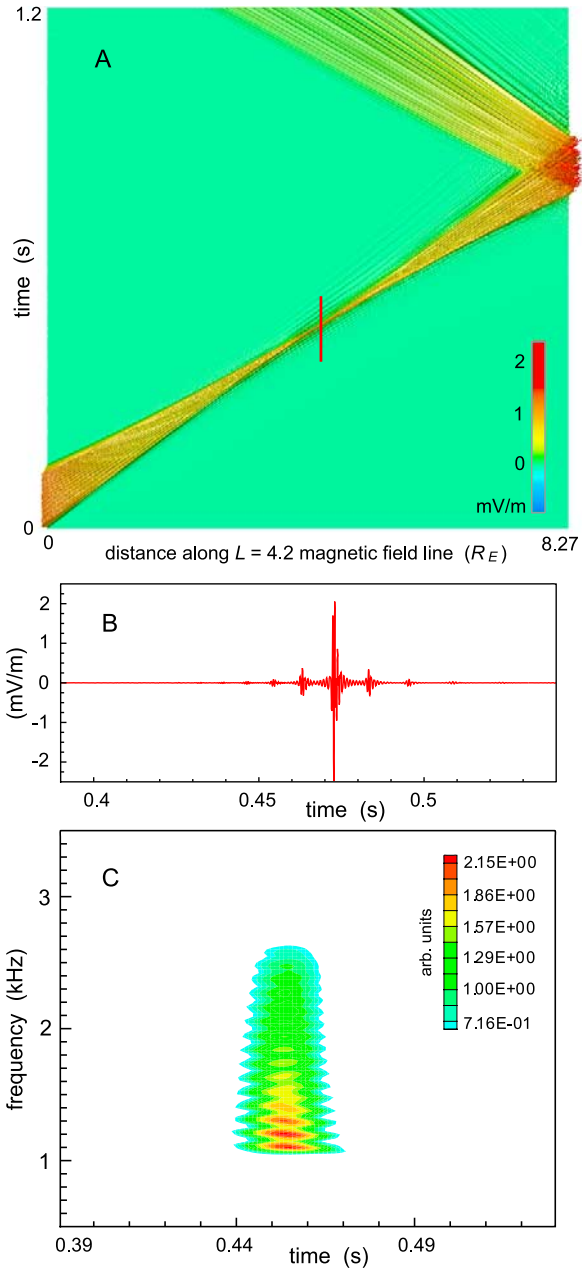

Figure 11. (a) Amplitude of E_y in the signal with a discrete frequency modulation. (b) E_y at the location shown with red line in Figure 11a. (c) Temporal variation of the amplitude spectra of E_y shown in Figure 11b.

than the window used to calculate spectrograms shown in Figure 8, the spectra shown in Figure 11c spread over a larger time interval than the spectra shown in Figure 8 (A2). The larger time window is used to get a better frequency resolution of the signal, which is important to demonstrate that the signal with a discrete frequency modulation can be compressed to a high-power signal with frequency gaps between different components. To answer the question if such a signal can be amplified in the equatorial magnetosphere by wave-particle interactions and cause secondary emissions, wave-particle simulations like the ones presented by *Streltsov et al.* [2009] and active experiments at HAARP need to be done.

6. Conclusions

[22] Results from our numerical simulations, based on the novel algorithm, solving one-dimensional EMHD equations in the dipole coordinate system, demonstrate that the amplitude (and power) of the whistler mode waves transmitted by the powerful HF transmitter can be significantly increased in the equatorial magnetosphere when this signal contains several frequency components distributed in time. To maximize the signal power at this particular location, these components should be transmitted with some time delays. For the parameters of the waves and the Earth's magnetosphere considered in this study, these time delays can be estimated from the dispersion relation for whistler mode waves. Simulations showed that the bandwidth of the transmitted wave does not change at different locations along the wave path within the time interval of the wave transmission; however, all frequency components of the transmitted signal arrive at the focusing point simultaneously, which leads to an appearance of a broadband signal at this location.

[23] The broadband format of the signal can play against its possible amplification by the wave-particle interactions at the equatorial magnetosphere. In this case, the signal containing several discrete frequencies with a gap of 100 Hz can be used. Such a signal also can be "compressed" in the chosen location along the ambient magnetic field line with almost the same efficiency as the continually modulated signal. We plan to investigate possible amplification of the signals with discrete and continuous formats of frequency modulation in future experiments at HAARP.

[24] **Acknowledgments.** The research was supported by the ONR MURI Award #528828 to the University of Maryland.
[25] Amitava Bhattacharjee thanks Michael Starks and Michael Rycroft for their assistance in evaluating this paper.

References

Angerami, J. J. (1970), Whistler duct properties deduced from VLF observations made with the ogo 3 satellite near the magnetic equator, *J. Geophys. Res.*, *75*, 6115.
Burden, R. L., and J. D. Faires (2001), *Numerical Analysis*, Brooks/Cole, New York.
Carpenter, D. L., and R. R. Anderson (1992), An ISSE/whistler model of equatorial electron density in the magnetosphere, *J. Geophys. Res.*, *97*, 1097.
Gołkowski, M., U. Inan, A. Gibby, and M. Cohen (2008), Magnetospheric amplification and emission triggering by ELF/VLF waves injected by the 3.6 MW HAARP ionospheric heater, *J. Geophys. Res.*, *113*, A10201, doi:10.1029/2008JA013157.
Gordeev, A., A. Kingsep, and L. Rudakov (1994), Electron magnetohydrodynamics, *Phys. Rep.*, *243*, 215.
Gurevich, A. (2007), Nonlinear effects in the ionosphere, *Phys. Uspekhi*, *50*, 1091.
Helliwell, R. (1965), *Whistlers and Related Ionospheric Phenomena*, Stanford Univ. Press, Stanford, Calif.
Helliwell, R. (1988), VLF simulated experiments in the magnetosphere from Siple station, Antarctica, *Rev. Geophys.*, *26*, 551.
Hobara, Y., V. Y. Trakhtengerts, A. G. Demekhov, and M. Hayakawa (2000), Formation of electron beams by interaction of a whistler wave packet with radiation belt electrons, *J. Atmos. Sol. Terr. Phys.*, *62*, 541.
Inan, U., and T. Bell (1977), The plasmapause as a VLF wave guide, *J. Geophys. Res.*, *82*, 2819.
Inan, U., H. Chang, R. Helliwell, W. Imhof, J. Reagan, and M. Walt (1985), Precipitation of radiation belt electrons by man-made waves: A comparison between theory and measurement, *J. Geophys. Res.*, *90*, 359.

Inan, U., T. Bell, J. Bortnik, and J. Albert (2003), Controlled precipitation of radiation belt electrons, *J. Geophys. Res.*, *108*(A5), 1186, doi:10.1029/2002JA009580.

Karpman, V. I., Y. N. Istomin, and D. R. Shklyar (1974), Nonlinear theory of a quasimonochromatic whistler mode packet in inhomogeneous plasma, *Plasma Phys.*, *16*, 685.

Kondrat'ev, I. G., A. V. Kudrin, and T. M. Zaboronkova (1999), *Electrodynamics of Density Ducts in Magnetized Plasmas*, Gordon and Breach, Amsterdam, Netherlands.

Koons, H. C. (1989), Observations of large-amplitude whistler mode wave ducts in the outer plasmasphere, *J. Geophys. Res.*, *94*, 15,393.

Kostrov, A. V., A. V. Kudrin, L. E. Kurina, G. A. Luchinin, A. A. Shaykin, and T. M. Zaboronkova (2000), Whistlers in thermally generated ducts with enhanced plasma density: Excitation and propagation, *Phys. Scripta*, *62*, 51.

Moullard, O., A. Masson, H. Laakso, M. Parrot, P. Décréau, O. Santolik, and M. Andre (2002), Density modulated whistler mode emissions observed near the plasmapause, *Geophys. Res. Lett.*, *29*(20), 1975, doi:10.1029/2002GL015101.

Nunn, D. (1974), A self-consistent theory of triggered vlf emissions, *Planet. Space Sci.*, *22*, 349.

Nunn, D., and A. J. Smith (1996), Numerical simulations of whistler-triggered vlf emissions observed in antarctica, *J. Geophys. Res.*, *101*, 5261.

Omura, Y., D. Nunn, H. Matsumoto, and M. J. Rycroft (1991), A review of observational, theoretical and numerical studies of vlf triggered emissions, *J. Atmos. Terr. Phys.*, *53*, 351.

Papadopoulos, K., T. Wallace, M. McCarrick, G. M. Milikh, and X. Yang (2003), On the efficiency of ELF/VLF generation using HF heating of the auroral electrojet, *Plasma Phys. Rep.*, *29*, 561.

Sazhin, S. (1993), *Whistler-Mode Waves in a Hot Plasmas*, *Cambridge Atmos. and Space Sci. Ser.*, Cambridge Univ. Press, Cambridge, U.K.

Scarf, F. L., and C. R. Chapell (1973), An association of magnetospheric whistler dispersion characteristics with changes in local plasma density, *J. Geophys. Res.*, *78*, 1597.

Stenzel, R. L. (1976), Whistler wave propagation in a large magnetoplasma, *Phys. Fluids*, *19*, 857.

Streltsov, A. V., W. Lotko, and G. Milikh (2005), Simulation of ULF field-aligned currents generated by HF heating of the ionosphere, *J. Geophys. Res.*, *110*, A04216, doi:10.1029/2004JA010629.

Streltsov, A., M. Lampe, and G. Ganguli (2007), Whistler propagation in non-symmetrical density channels, *J. Geophys. Res.*, *112*, A06226, doi:10.1029/2006JA012093.

Streltsov, A., E. Mishin, and G. Joyce (2009), Nonlinear interactions of broadband whistler waves with energetic electrons, *J. Atmos. Sol. Terr. Phys.*, *71*, 897–904, doi:10.1016/j.jastp.2009.02.007.

Trakhtengerts, V. Y., M. J. Rycroft, and A. G. Demekhov (1996), Interaction of noise-like and discrete ELF/VLF emissions generated by cyclotron interactions, *J. Geophys. Res.*, *101*, 13,293.

Trakhtengertz, V. Y., P. P. Belyaev, S. V. Polyakov, A. G. Demekhov, and T. Bösinger (2000), Excitation of Alfvén waves and vortices in the ionospheric resonator by modulated powerful radio waves, *J. Atmos. Terr. Phys.*, *62*, 267.

Trakhtengerts, V., A. Demekhov, E. Titova, B. Kozelov, O. Santolik, D. Gurnett, and M. Parrot (2004), Interpretation of Cluster data on chorus emissions using the backward wave oscillator model, *Phys. Plasmas*, *11*, doi:10.1063/1.1667495.

Trakhtengerts, V., et al. (2007), Formation of VLF chorus frequency spectrum: Cluster data and comparison with the backward wave oscillator model, *Geophys. Res. Lett.*, *34*, L02104, doi:10.1029/2006GL027953.

M. Gołkowski and U. S. Inan, STAR Laboratory, Stanford University, 350 Serra Mall, Stanford, CA 94305, USA. (mag41@stanford.edu; inan@stanford.edu)

K. D. Papadopoulos, Department of Physics, University of Maryland, John S. Toll Physics Building, College Park, MD 20742, USA. (dpapadop@umd.edu)

A. V. Streltsov, Thayer School of Engineering, Dartmouth College, 8000 Cummings Hall, Hanover, NH 03755, USA. (anatoly.v.streltsov@dartmouth.edu)